Fracture of Porous Materials Induced by Crystallization of Salt

by

Golda Y. Katzoff

B.S., Mechanical Engineering (2004)

Johns Hopkins University

Submitted to the Department of Civil and Environmental Engineering in
Partial Fulfillment of the Requirements for the Degree of

Master of Engineering in Civil and Environmental Engineering

at the

Massachusetts Institute of Technology

June 2006

Signature of Author.....
Department of Civil and Environmental Engineering
May 12, 2006

Certified by.....
Franz-Josef Ulm
Professor of Civil and Environmental Engineering
Thesis Supervisor

Accepted by.....
Andrew J. Whittle
Chairman, Departmental Committee on Graduate Students

Fracture of Porous Materials Induced by Crystallization of Salt

by

Golda Y. Katzoff

Submitted to the Department of Civil and Environmental Engineering
on May 12, 2006 in Partial Fulfillment of the Requirements for the Degree of
Master of Engineering in Civil and Environmental Engineering

ABSTRACT

The penetration of salt into porous materials is known to have deleterious effects, often resulting in fracture. The damage process begins with a saline solution penetrating the porous network by way of capillary action. This is followed by supersaturation of the saline solution, which may result in the formation of salt crystals. In turn, these salt crystals induce pressure on the pore walls. Though the stress generated by the crystallization of salt in a single pore alone is unlikely to result in fracture, if the crystallization region is large enough, the combined effects can lead to fracture.

This thesis will first provide an overview of the crystallization process and then focus on the factors leading directly to fracture. The thesis will examine various key processes proposed by researchers, identify elements that have not yet been explored, and finally propose a cohesive outline of the processes responsible for fracture.

Thesis Supervisor: Franz-Josef Ulm
Title: Professor of Civil and Environmental Engineering

Acknowledgements

The completion of this thesis marks the culmination of my two years at MIT. Two years that, without a doubt, were the most personally and academically challenging years of my life. I could not have made it to this point of graduating from this esteemed institution without the help and support of a number of people.

Firstly, I am most appreciative and indebted to my thesis advisor, Professor Franz Ulm, for his direction, his patience, his availability, and for relaying the confidence that I could tackle this difficult subject which, on more than one occasion, I feared was well beyond my realm of competence.

I'd also like extend my thanks to Dr. Eric Adams, for considering my transfer to the CEE M.Eng program on such short notice. And to my course advisor, Professor JJ Connor, for all the advice. And thank you to my M.Eng classmates (AKA, the moosheads) for filling me in on my deficient knowledge of civil engineering, and for your humor and comradeship.

I must express my acknowledgements to the National Science Foundation for awarding me their generous graduate fellowship.

And despite my arduous couple years at MIT, I'd like to express my sincere appreciation to my original advisor at MIT, Professor Raul Radovitzky, if not for whom, I most probably would have gone to an unnamed university in the Bay Area of California. I am most grateful to Raul for his being the first encouraging voice at MIT, for his recruiting efforts, and more importantly, for his understanding, and for bearing with me as I attempted to figure out what direction to take my education.

I am also very grateful to Leslie Regan, from the mechanical engineering graduate office, for being most helpful in facilitating both my coming to and adjusting to MIT. From the day I was admitted to MIT until my "departure" from the mechanical engineering department, Leslie has been extremely supportive, friendly, and just altogether fantastic.

Additionally, I am most obliged to all the professors (too many to list) that took the time to talk to me about their research and welcomed me to join their labs while I was exploring my interests. Thanks is due to as well to all the graduate students who candidly gave me the rundown on what it was really like doing research with a number specific professors.

Many thanks to my former labmates in EBM: Alex Thierez and Jeff Dahmus; and to all my labmates in Telac, my first lab at MIT, with special mention of those I shared a cubicle area with: Antoine Jerusalem, Daniel Tam, and Nathan Wicks. Thank you for your companionship, for all your coaching, and for encouraging me to explore other options in an effort to figure out what I want to do.

I might not have applied to MIT, or perhaps even graduate school, let alone won the NSF fellowship, if not for my undergraduate advisor, Professor Louis Whitcomb. I cannot believe my good fortune in having the most wonderful advisor a student could possibly hope for. Professor Whitcomb not only provided me with optimal direction through out my undergraduate years at Johns Hopkins, but he actually pushed me to excel well beyond my highest expectations, not allowing me to settle for anything less my best effort, and believing that I could achieve more than I myself could ever imagined I could. Furthermore, he served as constant inspiration for me as an example of a cutting edge researcher and a dedicated first rate teacher who was always available for his students.

I'd also like to acknowledge all of my other professors at Johns Hopkins for providing me with a superb education. Though I'm not sure it's possible to ever be adequately prepared for graduate school in the mechanical engineering department at MIT, I think Johns Hopkins brought me as close to being prepared as possible (in the academic sense at least). Special thanks to Professors Roger Ghanem, Jean-François Molinari, Allison M. Okamura, William N. Sharpe, Ilene J. Busch-Vishniac, and Dr Andrew Conn, for their advice and encouragement outside of the classroom.

I owe my sanity to all my friends who maintained contact despite my enrolling at MIT. Firstly, to the Lefferts Crew: Esty Kaminker, Tzipora Rivkin, and Bella Schapiro for their nearly two decades of friendship and contributing to who I am and to where I am today. I'm also particularly grateful to the friends who traveled to visit me in Cambridge: Michelle Clark, Chumi Lein, Pnina Levitz, and Shana Olidort, as well as to Greg Burton, Danielle Soya, and Brian Yagoda, for making a point to meet up with me when they were in town. And to my other friends who provided moral support from afar: Nava Chitrick, Miriam Fliegner, Liba Ginsburg, Francine Katz, Agatha Monzon, Kimberly Rosendorf, Dini Schwartz, Yaakov Shaul, Sarah Spinner, Soshie Weingarten, and anyone else I might have forgotten...

Finally, I'd like to thank my family, and my parents most of all for continually supporting me without reservation, despite my going on a track which is not necessarily encouraged by the community. I am especially grateful to my mother. Among countless other things, thank you so much for gladly putting up with my constant barrage of phone calls, and not only taking the time to listen to me, but making me realize, on a number of occasions, that my life wasn't ultimately falling apart for real this time, and things would work out somehow.

Table of Contents

Chapter 1

Introduction

1.1 Industrial Context

Historic preservation of structures is the effort to prevent historic structures from deteriorating and to maintain their architectural beauty along with their historical significance [3]. For optimal preservation and reconstruction, a scientific understanding of the deterioration mechanisms related to specific structures is essential. Indeed, when there is a lack in understanding, efforts aimed at preservation might result in actually increasing the damage to the structure.

Historic structures situated near the sea deteriorate at especially fast rates. The salt from the seawater, along with the humidity of the air, as well as sea-spray, create a particularly unfriendly environment to structures, especially those made of porous materials, like masonry, or concrete. Before attempts to preserve and/or restore these structures are made, first it is essential to develop an understanding of the deterioration mechanism at hand. Specifically, it is necessary to understand the stress and resulting fracture of porous materials due to the crystallization of salt in the pores of these structures. Once an understanding of the problem is achieved, corrective steps can be developed.

1.2 Background

The presence of water alone accelerates the decay of structures, and with the addition of salt, the rate of deterioration is further increased [8]. Salt water can penetrate porous materials by various means such as from rain water, through the air by condensation or mist, sea spray, or by capillary rise, when liquids climb up the surfaces of narrow spaces

[3]. Once the saline water has penetrated the pore space, both a temperature reduction and a higher concentration of salt in the solution due to evaporation can result in the formation of salt crystals due to supersaturation of the solution [1], [4], [8]. In turn, the crystallization of salt results in pressures against the pore walls, and if these stresses are large enough, fracture can occur.

A number of researchers have studied this problem of salt crystallization using various approaches [1], [4], [6], [8]. The free energies and work involved in stress and fracture have been developed through thermodynamic approaches [1], [4], [8], and experiments have been performed both to test theoretical derivations as well as to better understand the deterioration process [6].

1.3 Research Motivation

While much progress has been made in the efforts to understand the mechanisms behind the crystallization of salt in porous materials and the resulting fracture, there are still many aspects of the problem that remain unexplored. The objective of this thesis is to provide a better understanding of when and how fracture occurs in porous materials due to the crystallization of salt by giving a clear overview of what researchers in this field have discovered, examining the different approaches taken in predicting fracture, and then syndicating the various conclusions and determining the factors that have not yet been fully investigated.

1.4 Thesis Outline

This thesis is divided into six chapters. It begins by providing a thermodynamic formulation of crystallization of salt in porous materials in Chapter two. The third chapter follows with an overview of some of the experimental research related to salt crystallization. Chapter four is a step-by-step overview of the crystallization process beginning from penetration of saline solution to fracture. The conditions leading to fracture are then delved into in more depth in Chapter 5. Finally, Chapter 6 contains conclusive remarks including suggestions for future research as well as applications for preservationists.

Chapter 2

Thermodynamic Background

2.1 Introduction

This chapter reviews the thermodynamic model of crystallization of salt in porous matter proposed by Coussy [1].

2.2 Thermodynamics of Confined Crystallization

The thermodynamics of the crystallization of salt in a porous material can be analyzed with the help of poromechanics, the study of the behavior of porous materials that are comprised of a porous "skeleton" (or solid matrix) and fluids saturating the pores [10]. A saline solution infused in masonry would be characterized in the context of a non-saturated or unsaturated poroelasticity saturated by three fluid phases: a gaseous phase, G, a liquid phase, L, and a (solid) crystal phase, C [1].

The porous material can be divided into two parts, the skeleton, and the porous space saturated by the different phases. The free energy of the skeleton can be expressed with the help of the Clausius-Duhem inequality given as [1]:

$$\sigma_{ij} d\varepsilon_{ij} + \sum_{J=G,L,C} p_J d\phi_J - dF_{sk} \geq 0, \tag{1}$$

where F_{sk} is the Helmholz free energy of the skeleton, $\sigma_{ij} d\varepsilon_{ij}$ represent the strain work rate related to deformation of the overall material, p_J and $d\phi_J$ represent the pressures and change in porosity the different phases, j=G,L,C, occupy.

The above formulation accounts for both the skeleton deformation and the changing interfaces between phases, with the changing porosities $d\phi_J$ resulting from two separate processes. The first is the process of the pore space being invaded by the saline solution, a gaseous mixture, and the solid crystal, which creates new interfaces between the skeleton and the fluids saturating the pore space. The second process accounts for deformation of the skeleton only due to pressures on the pore walls from the solution, gas, and crystals saturating the porous network. Thus the partial porosities, ϕ_j, can be split into two independent parts as such:

$$\phi_j = \phi_0 S_J + \varphi_J; \qquad S_C + S_L + S_G = 1, \tag{2}$$

with $\phi_0 S_J$ representing the first process (ϕ_0 is the initial overall porosity and S_J is the saturation), while φ_J is limited to accounting for change in porosity due to the skeleton deformation only. Thus, current overall porosity only involves skeleton deformation and is given by:

$$\phi = \phi_0 + \sum_{J=G,L,C} \varphi_J \,. \tag{3}$$

Now, assuming elastic behavior of the skeleton as well as ignoring irreversible effects related to the invasion process, the dissipation can be set equal to zero to get the following equality from Equation (1):

$$\sigma_{ij} d\varepsilon_{ij} + \sum_{J=G,L,C} p_J d\phi_J - dF_{sk} = 0 \,. \tag{4}$$

From the above equality, the unsaturated poroelastic state equations are recognized:

$$F_{sk} = F_{sk}(\varepsilon_{ij}, \phi_J); \qquad \sigma_{ij} = \frac{\partial F_{sk}}{\partial \varepsilon_{ij}}; \qquad p_J = \frac{\partial F_{sk}}{\partial \phi_J}. \tag{5}$$

The difficulty of the state equations written in the form of (5) is that it is difficult to link them to results obtained from experiments, where there are separate energies for the skeleton deformation and the creation of new interfaces. To overcome this difficultly, the free energy $F_{sk} = F_{sk}(\varepsilon_{ij}, \phi_J)$ is divided into two parts: the first limited to describing the energy contribution from skeleton deformation, while the second part would consist of the energy required to create new interfaces. The free energy first must be expressed with the variables involved with both energy processes in the form:

$$F_{sk}(\varepsilon_{ij}, \phi_J) = \Psi_{sk}(\varepsilon_{ij}, \varphi_J, S_C, S_G). \tag{6}$$

Now using Equation (6), the state equations given by Equation (5), and the relation between porosities (2), the state equations can be rewritten in the form:

$$\sigma_{ij} = \frac{\partial \Psi_{sk}}{\partial \varepsilon_{ij}}; \qquad p_J = \frac{\partial \Psi_{sk}}{\partial \varphi_J}; \tag{7}$$

$$\phi_0(p_C - p_L) = \frac{\partial \Psi_{sk}}{\partial S_C}; \qquad \phi_0(p_G - p_L) = \frac{\partial \Psi_{sk}}{\partial S_G}. \tag{8}$$

While the energy balance now becomes:

$$\sigma_{ij} d\varepsilon_{ij} + \sum_{J=G,L,C} p_J d\varphi_J + \phi_0(p_C - p_L) dS_L + \phi_0(p_G - p_L) dS_G - d\Psi_{sk} = 0. \tag{9}$$

The first two terms of (9) relate to the work rate of the deformation of the solid skeleton, while the 3rd and 4th terms represent the infinitesimal work done against interfacial forces.

It is also useful to divide the free energy of the skeleton into 2 parts. The first part representing the elastic free energy of the porous solids is given as W, and the second part representing the surface energy of interfaces as U. This eventually leads to the state equations given as:

$$\sigma_{ij} = \frac{\partial W}{\partial \varepsilon_{ij}}; \qquad p_J - p_0 = \frac{\partial W}{\partial \varphi_J}. \tag{10}$$

Or by introducing the Legendre-Fenchel transform W^* of W with respect to φ_J one obtains the state equations in the form:

$$\sigma_{ij} = \frac{\partial W^*}{\partial \varepsilon_{ij}}; \qquad \varphi_J = \frac{\partial W^*}{\partial (p_J - p_0)}. \tag{11}$$

Finally, the elastic energy, W, stored within the solid matrix can be written in the form:

$$W = \frac{1}{2}\frac{\left(\sigma + \sum_{J=G,L,C} b_J (p_J - p_0)\right)^2}{K} + \frac{1}{2}\sum_{J,K=G,L,C} \frac{(p_J - p_0)(p_K - p_0)}{N_{JK}} + \frac{1}{2}\frac{s_{ik}s_{kj}}{G}, \tag{12}$$

where K is the bulk modulus, G is the shear modulus, b_J and N_{JK} are the Biot coefficient and the Biot Modulus, and σ and s_{ij} represent the mean stress and the deviatoric stress respectively given by:

$$\sigma = \frac{1}{3}\sigma_{kk}; \qquad s_{ij} = \sigma_{ij} - \sigma\delta_{ij}. \tag{13}$$

2.3 Summary

The thermodynamic approach proposed by Coussy [1] separates the deformation of the solid from interfacial affects occurring in the pore space or at the fluid-solid interface. This is done in an effort to provide a bridge between the poromechanics theory devoted to the deformation of porous media and the experimental physical chemistry approaches which will be discussed in the forthcoming chapters.

Chapter 3

Experimental Results

3.1 Introduction

Experiments simulating the crystallization of salt are useful as an illustration of the damage penetration of salt in porous materials can induce. Furthermore, experiments are essential both to verify already developed theories, as well as to provide guidance to inspire new theories. A brief review of some of the experimental work related to crystallization of salt is presented in this chapter.

3.2 Pore Size

Rodriguez-Navarro and Doehne [6] studied the microscale as well as macroscale characteristics of limestone saturated with sodium sulfate and sodium chloride. Their experiments provided valuable insight into the damage of salt in porous materials in general, but their conclusions on the effects of pore size and pore distribution to crystallization are of particular interest. They found that materials with a high proportion of micropores were susceptible to more damage than materials with larger pores. They postulate that this is because the micropores result in a larger surface area causing solution to flow more slowly in a network, causing crystallization to occur both deeper in the stone, which is shown to be more harmful [8]. They also discuss how in a network of pores crystallization will occur first in the smaller pores, with larger pores supplying solution for the crystallization process occurring in the smaller pores. Rodriguez-Navarro also shows that damage was largely a function of supersaturation ratio x/x_0.

3.3 Efflorescence vs. Subflorescence

Scherer [8] did experiments that demonstrated the harmful effects of crystallization of salt, and also distinguished between level of damage done by efflorescence, the growth of the salt on the surface, versus subflorescence, which is the crystallization of salt beneath the surface or within the porous network. Scherer's experiments involved samples of prismatic stone suspended with their bottoms' touching a solution of sodium sulfate. Gravity was assumed to be negligible since the samples were short in height. The rise in height of the saline solution is given by [8]:

$$h = S\sqrt{t}\,, \tag{14}$$

where S, the sorptivity or the capacity of the medium to absorb liquid by capillary rise, is given by:

$$S = \sqrt{\frac{2kp_c}{\eta}}\,, \tag{15}$$

where the permeability k is roughly proportional to the square of the pore size; the capillary pressure p_c is proportional to the inverse of the pore size, and η is the viscosity. Two samples were tested: sample 1 was a sandstone sample with a porosity of 0.21 and sorptivity of 0.18 cm/s$^{1/2}$; while sample 2 was limestone sample, with the same porosity as sample 1, but less permeable, with a sorptivity of 0.06 cm/s$^{1/2}$.

The experimental results revealed the bottom half of sample 1 to be covered in growth of salt crystals growing on the surface (efflorescence), while the top half suffered from subflorescence, where the salt crystallized inside the pores. Sample 2 showed no signs of efflorescence. Subflorescence was shown to be more damaging than efflorescence, with cracks appearing on the surface of the limestone after just 8 days; and after 47 days, a 2 mm layer separating from the surface of the block (see Figure 1). These results verify that smaller pore size (such as that of limestone compared to sandstone) in material is prone to more damaging effects by salt crystallization.

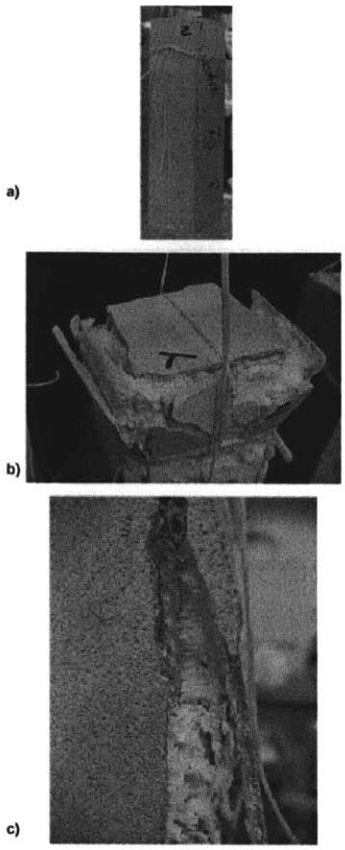

Figure 1: Sample of limestone where (a) is the sample after 8 days and shows signs of cracking, (b) is the sample after 47 days and a layer of stone has separated from the surface, and (c) is a closer view of the (b) [8].

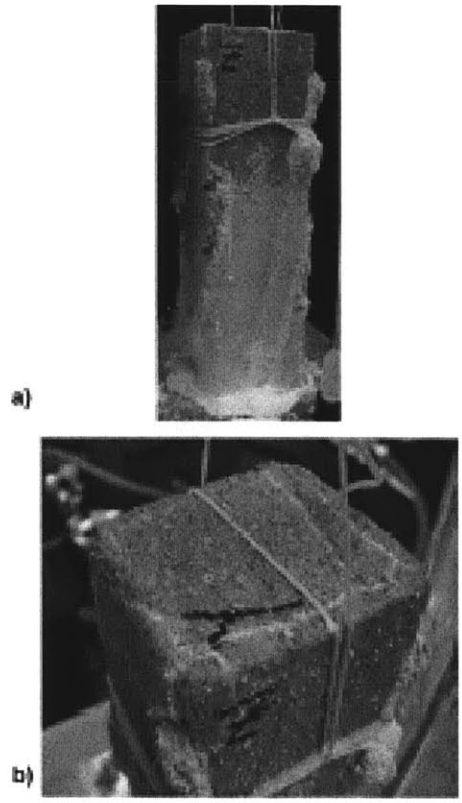

Figure 2: Sample of sandstone demonstrating efflorescence on the bottom half (a), and cracking due to subflorescence on the top (b), after 47 days of exposure to sodium sulfate [8].

3.4 Phases of Sodium Sulfate

Sodium sulfate is the most damaging of salts, and has been found to cause damage even in the absence of evaporation. Flatt [4] provides an overview of the experiments demonstrating the properties of sodium sulfate. It can exist in two stable phases at room temperature: in the anhydrate form as thenardite, and in the decahydrate form as mirabilite [4], [8]. At 93% relative humidity, the saturated solution is in equilibrium, but as the humidity decreases to 75% (at 20°C), a phase transition is observed to occur as the mirabilite becomes less stable than the thenardite. Furthermore, sodium sulfate becomes unstable at temperatures above 32°C, but as the temperature drops below 32°C, the range of humidity at which it is stable increases. Thenardite is also observed to change to mirabilite with an increase in humidity. The phases of sodium sulfate with respect to temperature are shown in Figure 3.

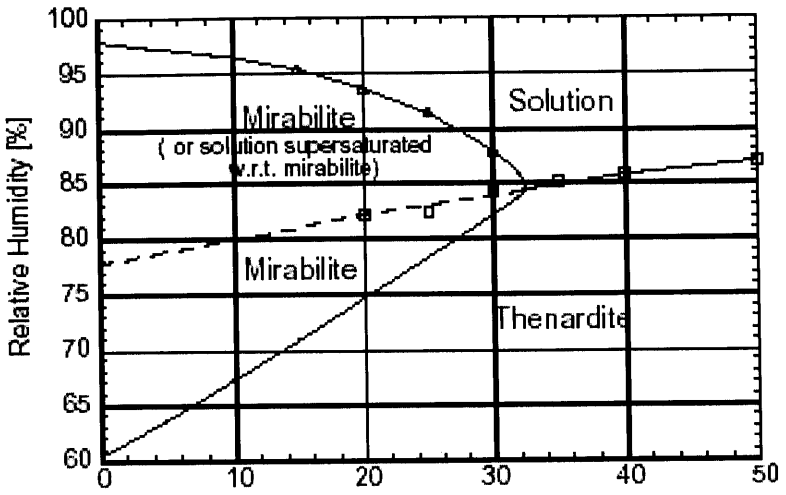

Figure 3: Phase diagram for sodium sulfate where the continuous lines represent boundaries of the stable phases [4].

3.5 Summary

The experimental results presented in this chapter demonstrate the damaging effects crystallization of salt can have on porous materials. Furthermore, the results isolate the effects of certain factors, such as pore size, in the crystallization process. These factors will be quantified and integrated into the theoretical research in the next two chapters.

Chapter 4

The Crystallization Process

4.1 Introduction

This chapter provides a review of the phenomena involved in the process of crystallization of salt in porous materials. The process begins with the deposition of saline solution on the porous material by various means. Then the solution is absorbed into the material by capillary action. Next supersaturation can occur, and crystal growth may result, which generates stresses on the pore walls. Finally, if crystallization spreads through an adequate volume, fracture will occur. Figure 4 displays a flow chart of the steps leading to fracture. The question mark is in reference to what occurs after stresses are induced by crystallization and before fracture occurs. This step is introduced in the last section of this chapter, and is fully developed in Chapter 5.

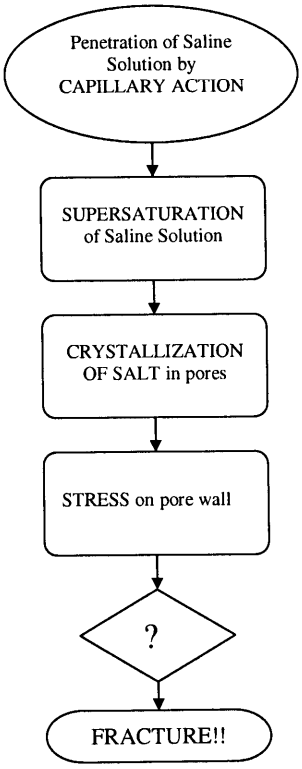

Figure 4: Flow chart of crystallization of salt.

4.2 Deposition of Saline Solution

There are a number of ways water can end up in the porous materials of a structure. For instance, water can enter the porous material directly from rainfall, from dripping from roof onto the walls of the structure, or from sea spray. If the material is in contact with the soil, water can be drawn up from the soil into the pores.

4.3 Capillary Action

Once the water is on the porous material, it can be suctioned into the pores by capillary effects. The force driving capillary rise is the capillary pressure, p_c, and it depends on the wetting properties of the porous material as well as the pore size distribution. The rate of flow, or flux, from capillary rise from the ground, is given by [8]:

$$J_c = \phi A \frac{dh}{dt} = \frac{k}{\eta} \frac{(-p_c - \rho_l g h)}{h}, \tag{16}$$

where k is the permeability of the porous material, and η is the viscosity, A is the area of the surface in contact with the ground, h is the height the liquid has risen to, and ϕ is the porosity of the material. One can see from Equation (16) that as the liquid height increases, the rate of flow decreases. However, the rate of evaporation remains constant, which means that at some point, the evaporation rate will exceed the rate of capillary rise and the liquid will stay at some constant height.

When capillary rise involves a saline solution as opposed to water, things get more complicated. When water evaporates from the solution, it will result in a higher concentration of salt of the liquid near the drying surface relative to the salt concentration of the rest of the liquid. In order to comply with the laws of entropy, this concentration gradient results in the movement of the salt back towards the ground [8]. However, at greater heights, the gradient flattens out as the source is at a greater distance, and thus the salt concentration continually increases and supersaturation could eventually be reached.

4.4 Supersaturation of Solution

The supersaturation of a saline solution describes the chemical state of the solution that contains a higher concentration of salt than could remain dissolved in the solution under the existing conditions. The point at which a saline solution reaches supersaturation depends on a number of factors including the nature of the salt, the rate at which salt is supplied to the solution, and the degree of evaporation [8]. The supersaturation of a saline solution can result in the growth of salt crystals in a porous network.

4.5 Crystal Growth and Associated Pressure

The growth of crystals in a saline solution occurs when there is a difference in chemical potential between the crystal and the liquid. The chemical potential is given by [7]:

$$\Delta\mu = R\,T\ln(\frac{C}{C_0}), \tag{17}$$

where R is the ideal gas constant, T is the temperature, C is the concentration of the solute, and C_0 is the equilibrium concentration. If C is greater than C_0, the solution is supersaturated. In order to suppress growth of crystals, a hydrostatic pressure would have to be applied to the crystal [7]:

$$p_c = p_l + \frac{RT}{v_c}\ln(\frac{C}{C_0}), \tag{18}$$

with v_c signifying the molar volume of the crystal.

It has been estimated that pressures on the order of 30 MPa would be required to suppress crystal growth for a sodium chloride solution that is supersaturated by a factor of 2 at a temperature of 20°C [7].

For a crystal to grow into a pore, it is necessary that the contact angle between the crystal and the pore wall to be smaller than θ = 90° at the melting temperature of the crystal. Furthermore, for contact angles greater than θ = 90°, the smaller the pore, the lower the temperature required for crystal growth in the pore, as given by [7]:

$$\Delta T \approx -\frac{2\gamma_{cl}\cos(\theta)}{r_p \Delta S_{fv}}, \tag{18}$$

where γ_{cl} is the interfacial energy between the crystal and the liquid, r_p is the radius of the pore, and $\Delta S_{fv} = (S_L - S_C)/v_C$ is the entropy of fusion per unit volume. The shape of the crystal invading the pore is shown in Figure 5.

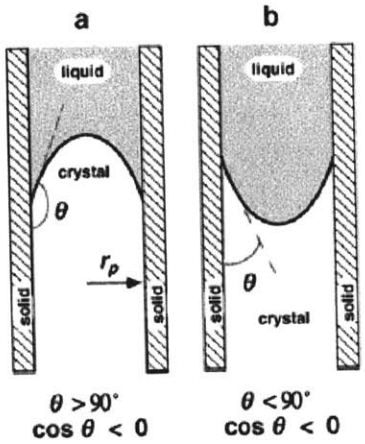

Figure 5: Crystal shape entering a cylindrical pore with radius r_p and contact angle (a) $\theta > 90°$; (b) $\theta < 90°$ [7].

Substantial energy is required before direct contact can occur between salt and the pore wall. This energy results from strong molecular forces such as van der Waals forces as well as electrostatic forces. This energy mismatch that exists between crystal and pore wall has to be overcome by a crystallization pressure in order for dry contact to occur between the crystal and the pore wall. If dry contact would occur, the crystal growth would be halted. However, dry contact requires a crystallization pressure be reached, and below this pressure, a thin liquid film exists between the crystal and the wall. From this thin film, ions feed crystal growth against the wall [4]. The pressure that prevents the crystal from growing towards the dry wall is the disjoining pressure, and is given by [4]:

$$P_d = \frac{2\gamma_{cl}}{r_p - \delta}, \tag{19}$$

where δ is the thickness of the liquid film that persists between the crystal and the pore wall. An increase in the interfacial energy between the crystal/liquid interface, γ_{cl}, results in slowing the process of crystal growth [8].

Flatt [4] extends the work of Scherer [7], [8] presenting the thermodynamic development of crystal growth of concentrated solutions of electrolytes, ultimately linking crystallization pressure to supersaturation with the following relation:

$$\gamma_{cl}\kappa_{cl} = -\frac{RT}{v_c}\left[\begin{array}{l}\left(\dfrac{1-x\sum_{i(C)}\alpha_i}{x}\ln(a_{s,H_2O})\right)_{x_0}^{x_f} + \int_{x_0}^{x_f}\dfrac{\ln(a_{s,H_2O})}{x^2}dx \\ +\dfrac{1}{v_l}\left(\left(\dfrac{m_1}{1+m_2x} - (v_c - v_l\sum_{i(C)}\alpha_i)\right)\ln(a_{s,H_2O})\right)_{x_0}^{x_f} + \dfrac{m_1m_2}{v_l}\int_{x_0}^{x_f}\dfrac{\ln(a_{s,H_2O})}{(1+m_2x)^2}dx\end{array}\right], \quad (20)$$

where v_c is the molar volume of the crystal , x is the molar fraction, x_0 is the solubility, and a_{s,H_2O} is the water activity.

Coussy [1] builds on the work of Flatt [4] to include the combined effects of the relative humidity and dilation effects in the crystal solute-solid equilibrium condition as given by:

$$p_C - p_L = \frac{RT}{v_C}\ln\left[\left(\frac{h_R}{1-Nx}\right)^{\frac{\delta v_C}{v_W}}\left(\frac{x}{x_0}\right)^N\left(\frac{1-Nx}{1-Nx_0}\right)^{v_w}\right], \quad (21)$$

where p_C is the crystallization pressure, p_L is the liquid pressure, h_R the relative humidity, N a stoichiometric value (3 for Mirabilite), x_0 is the solubility of the fluid, and δ the dilation coefficient. The molar fraction as a function of relative humidity can be obtained by numerically solving (see Appendix A for Matlab code) [1]:

$$\left(\frac{h_R}{1-Nx}\right)^{\frac{v_C}{v_W}(\delta+\frac{\gamma_{CL}}{\gamma_{GL}})}\left(\frac{x}{x_0}\right)^N\left(\frac{1-Nx}{1-Nx_0}\right)^{v_w} = 1. \quad (22)$$

One could also obtain the crystallization pore entry radius as a function of the molar fraction, given by [1]:

$$\frac{1}{r} = \frac{RT}{2v_C(\gamma_{CL}+\delta\gamma_{GL})}\ln\left[\left(\frac{x}{x_0}\right)^N\left(\frac{1-Nx}{1-Nx_0}\right)^{v_w}\right]. \quad (23)$$

The molar fraction as a function of humidity and the radius as a function of humidity are plotted in Figure 6.

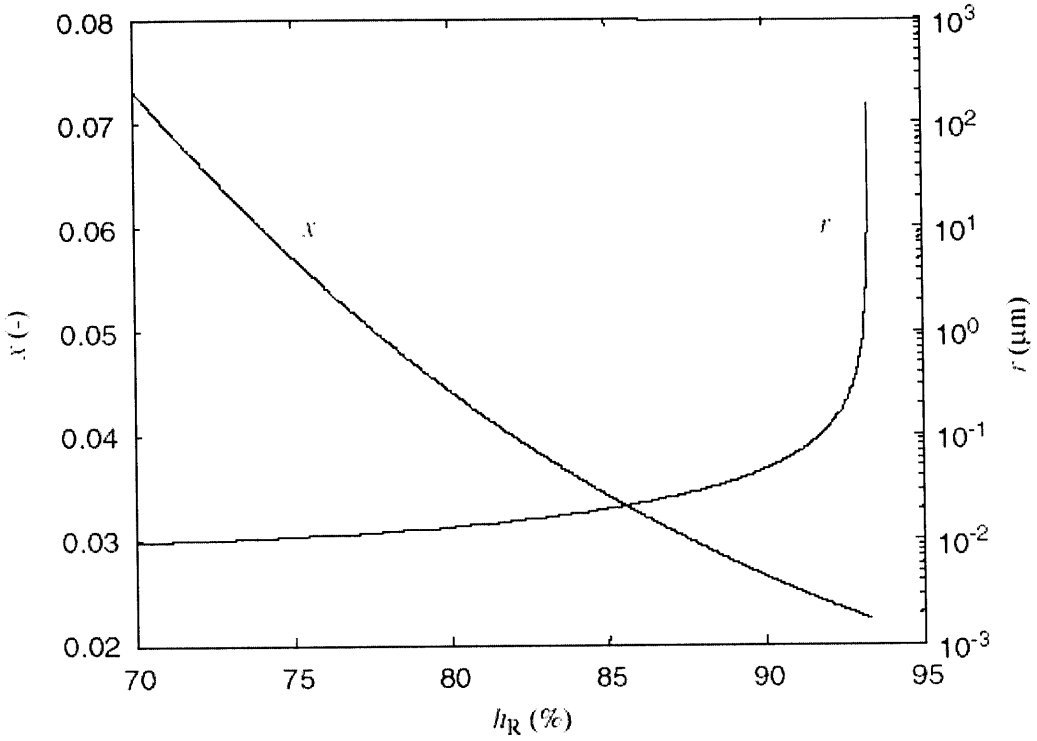

Figure 6: Molar fraction x and pore entry radius r plotted as functions of relative humidity [1].

4.6 Stress Resulting from Crystal Growth

The presence of a salt crystal in a pore results in a radial stress on the walls of the pore. The magnitude of this stress depends on γ_{sl}, the interfacial energy at the solid-liquid boundary, γ_{cl}, the interfacial energy at the crystal-liquid boundary, the radius of the pore, r_p, the contact angle, θ, and the pressure in the liquid p_l, and is given by [7]:

$$\sigma_r = \frac{\gamma_{cl}\cos(\theta)}{r_p} + \frac{\gamma_{sl}}{r_p} - p_l . \tag{24}$$

The greatest compression is found to occur at a contact angle of $\theta = 180°$ and can be expressed as [7]:

$$\sigma_r = \frac{\gamma_{sl}}{r_p} - \frac{\gamma_{cl}}{r_p - \delta} - p_l, \theta = 180°. \tag{25}$$

From the above equations, it is found that the crystal stress is linked to the size of the pores where crystal growth occurs, with smallest pores generating the largest pressures [4]. Furthermore, the growth of a large crystal into a pore with a small entry radius results in the maximum pressure on a pore wall [8].

The compressive radial stress as given by Equation (25) is counteracted by a tensile hoop stress in the pore wall, σ_θ. This hoop stress is ultimately what causes the most damage since masonry and concrete are weaker in tension than compression. By representing the pore as a cylindrical tube with inner radius r_p, outer radius b, and porosity given by $P=(r_p/b)^2$, the hoop stress is given by:

$$\sigma_\theta = -\sigma_r \left(\frac{1+P}{1-P} \right), \tag{26}$$

where σ_r is given by Equation (25). From Equation (26) one can deduce that if the porosity is small, the hoop stress is close in magnitude to the radial stress, and furthermore, that the tensile stress increases with an increase in porosity.

4.7 Propagation of Crystallization and Fracture

In Section 4.6 it was shown that the pressures induced by crystal growth can result in the development of high stresses on the pore wall. These stresses often exceed the tensile strength of the stone they act on, which is usually on the order of 3-9 MPa. However, a single pore encompasses too small a volume for the stresses from that pore alone to cause fracture. This is because in porous materials, such as masonry or concrete, the minimum size of a flaw that would result in cracking is much larger than the average pore size. This

critical flaw size, c, is given by the relation between the critical stress intensity of a material, K_{Ic}, the stress at failure, σ_A, [8]:

$$K_{Ic} \approx \sigma_A \sqrt{\pi c}. \tag{27}$$

Hence, for the stress generated by crystallization of salt in pores to cause significant damage, it is necessary that the crystals propagate through a considerable number of pores or volume of the material. The minimum tensile stress that could lead to propagation of flaws was studied in the context of concrete, and is given by the following relation [8]:

$$\sigma_\theta = \sqrt{\frac{8}{\pi}}\left(1+\frac{c}{R}\right)^{\frac{3}{2}} \frac{K_{Ic}}{\sqrt{c}}, \tag{28}$$

where R is the radius of the region where the stress is being generated, and c is the size of the flaw in an adjacent region, shown in Figure 7.

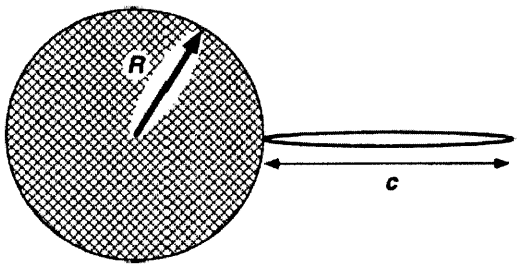

Figure 7: Flaw of length c adjacent to a region of radius *R* [8].

Figure 8 shows that for values of *R/c* that are less than ½, the hoop stress is small. Thus, unless salt crystals spread through a region comparable in size to the largest flaw size (which is much larger than average pore size), crystallization pressures will not cause local damage. Furthermore, even if crystallization occurs in a relatively large pore, the propagation of crystallization to other pores will be hampered by frequent constrictions.

In order for crystal growth to persist, the driving force must be great enough to allow it to pass through the breakthrough radius, r_{BT}, or the largest opening leading to other pores.

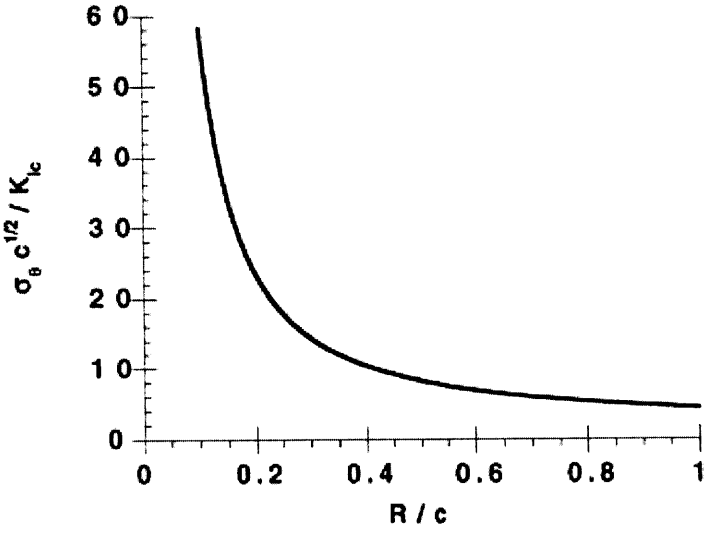

Figure 8: Normalized hoop stress that would cause growth of flaw as a function of the relative size of the flaw and region of stress [8].

Hence, since for fracture to occur the crystallized region has to be large enough to interact with the largest flaw, as given by Equation (27), and in order for the crystallization region to get that large, it is necessary that the driving force be sufficiently large as to allow the crystals to propagate through the porous network. This is governed by the crystallization process, which in turn requires a supersaturation given by [7]:

$$\frac{C}{C_0} \approx \exp\left[-\frac{2\gamma_{cl}\cos(\theta)}{r_{BT}}\left(\frac{v_c}{RG}\right)\right]. \tag{29}$$

Furthermore, these supersaturations must persist despite the natural tendency of the system to resist them.

4.8 Summary

The process of crystallization of salt was presented in this chapter, however, there remains the question of how exactly the process results in fracture. Scherer [8] proposes that first supersaturation must be attained for crystallization of salt to be initiated in the pore space. In addition, these supersaturations must persist so as to permit the propagation of crystallization. And finally, only once a region comparable in size to the critical size of a flaw has been invaded by salt crystals will the crystallization stresses be acting on a large enough region to generate fracture. The next chapter will delve into the conditions that lead to the proliferation of crystallization through the pore space that ultimately cause fracture.

Chapter 5

Fracture due to Crystallization

5.1 Introduction

The previous chapters provided a background of the phenomena at stake that lead to the fracture of porous materials due to crystallization of salt. While the analysis of the steps in the crystallization process have been relatively straightforward, with the researchers building on the conclusions developed in previously published papers, when it comes to quantifying the processes that directly lead to fracture, the research splits, with individual researchers focusing in on different factors, leaving a fragmented picture of what specifically causes fracture. Furthermore, some elements have not been explored by any of the researchers.

Scherer [8] provides a starting point for the fracture process by stressing that for fracture to occur, first it is necessary for crystallization to spread through a large enough volume of the porous network. The driving force that propels invasive crystallization of salt through large portions of the porous network is the pervasiveness of highly supersaturated solutions. The question Scherer [8] left somewhat open-ended is how these supersaturated solutions are achieved and maintained.

Flatt [4] evaluates how temperature variations can ultimately lead to highly supersaturated solutions which would lead to fracture. Coussy [1] on the other hand, focuses on changes in humidity, ultimately attributing fracture to the stresses induced by repeated imbibition-drying cycles.

In the sections that follow, each of the different approaches will be elaborated on, the weaknesses pointed out, and then the discrepancies between them as well as an approach to unify them are discussed.

5.2 Temperature as an Agent in Fracture

5.2.1 The Premise

Flatt [4] shows how supersaturation is highly dependent on temperature, as can be seen from Figure 9, x_0 is shown to vary as a function of temperature. Furthermore, with supersaturation being almost a direct link to eventual fracture, Figure 10 shows that drops in temperature result in increased stress.

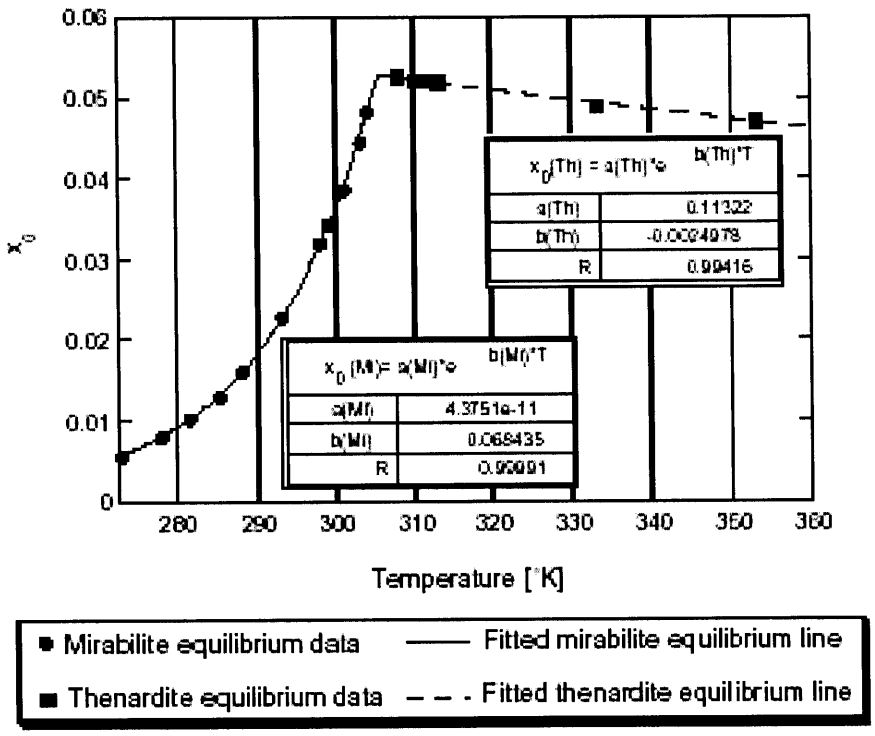

Figure 9: Solubility of thenardite and mirabilite versus temperature [4].

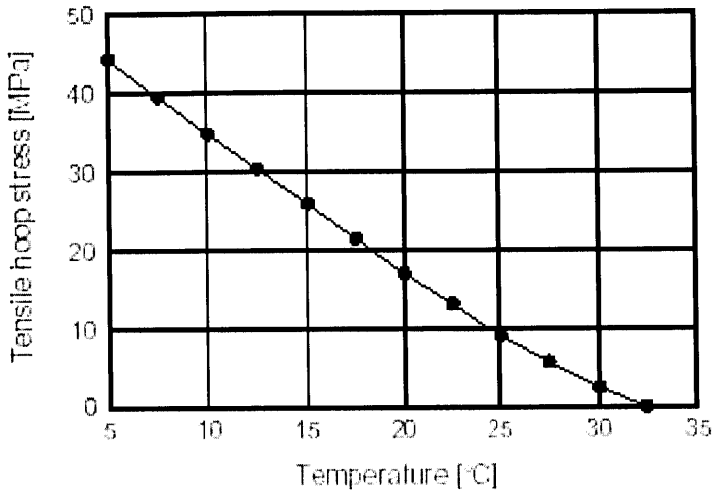

Figure 10: Tensile hoop stress versus temperature during impregnation of a thenardite containing stone in a saline solution [4].

Supersaturation occurs when sodium sulfate invades the material and then dries out in the conditions that allow thenardite to form (see Figure 3) [4]. The reduction of thenardite to liquid occurs the next time water enters the stone, and it results in quick supersaturation with respect to mirabilite. Though supersaturation can also occur by evaporation, since it raises the solution concentration by removal of water, it was found that adding ions to the solution by dissolution of thenardite is much more harmful than the drying out of the pores [4]. This lines up with other experimental results showing that most of the damage occurs during the impregnation step [4].

5.2.2 Open Question

Though Flatt [4] demonstrates that temperature and evaporation drops can lead to highly supersaturated solutions, he fails to provide a direct formulation that links these processes to fracture.

5.3 Imbibition-Drying Cycles

5.3.1 The Premise

It has been shown that the stresses in individual pores are not large enough to cause fracture [4], [5]. Thus, crystallization of salt has to propagate through many pores of the material before significant damage can occur. Coussy [1] proposes that this growth

process is facilitated by imbibition-drying cycles: with each new invasion of fluid to the system and the drying period that follows, crystallization stresses are induced. In his formulation of the critical stress that would lead to fracture, Coussy [1] highlights the effects of pore distribution, pore size, the tensile strength, as the factors that determine the ultimate resistance of the stone to weathering.

Coussy [1] devised a scheme to predict crystal, liquid, and gas saturations (denoted by S_C, S_L, and S_G respectively) during successive imbibition-drying cycles as given by the following equations:

$$\frac{S_C}{v_C} + \frac{xS_L}{v_L(x)} = \frac{x_{inv}^n}{v_L(x_{inv}^n)}; \tag{30}$$

$$\frac{x_{inv}^n}{v_L(x_{inv}^n)} = \frac{x_{inv}^1}{v_L(x_{inv}^1)}(1 - S_C^{n-1} - S_L^{n-1}) + \frac{S_C^{n-1}}{v_c} + \frac{x_{n-1}S_L^{n-1}}{v_L(x_{n-1})}, \tag{31}$$

where x_{inv}^1 is the molar fraction of the invading solution; x_{inv}^n is the molar fraction of the solution saturating the porous network after the nth complete imbibition; S_C^{n-1}, S_L^{n-1}, x_{n-1} are the saturations and molar fraction of the solution at the end of the (n-1)th drying period; and $v_L(x)$ is the molar volume of the liquid as given by:

$$v_L = v_W + x[(1+\delta)v_C - (N + \nu_w)v_W], \tag{32}$$

where, v_C, v_W are the molar volumes of the crystal and water, ν_w and N are stoichiometric constants of water, and δ is the dilation coefficient.

Before the next drying period, the actual crystal and liquid saturations, S_C and S_L, can be obtained by solving Equations (23), (30) and [1]:

$$S_L = S(r_h), \tag{33}$$

where r_h given is the largest entry radius (see Figure 11 for a plot of S_L as a function of radius), as well as imposing the constraint that there is no air left after the end of the

imbibition process given by $S_L=1-S_C$. During the nth drying period, x, S_C, and S_L as functions of the relative humidity can be obtained by solving Equations (22), (23), (30), and (33). And S_G can be obtained from $S_G=1-S_L-S_C$, since the three saturations have to total to one (see Equation (2)). The invading molar fraction is assumed to be a constant and is given by $x_{inv}^1 = 0.25x_0$ where x_0 is the solubility of mirabilite at a given temperature (Coussy assumes a constant temperature of 20°C for which $x_0=0.0235$ as shown in Figure 9).

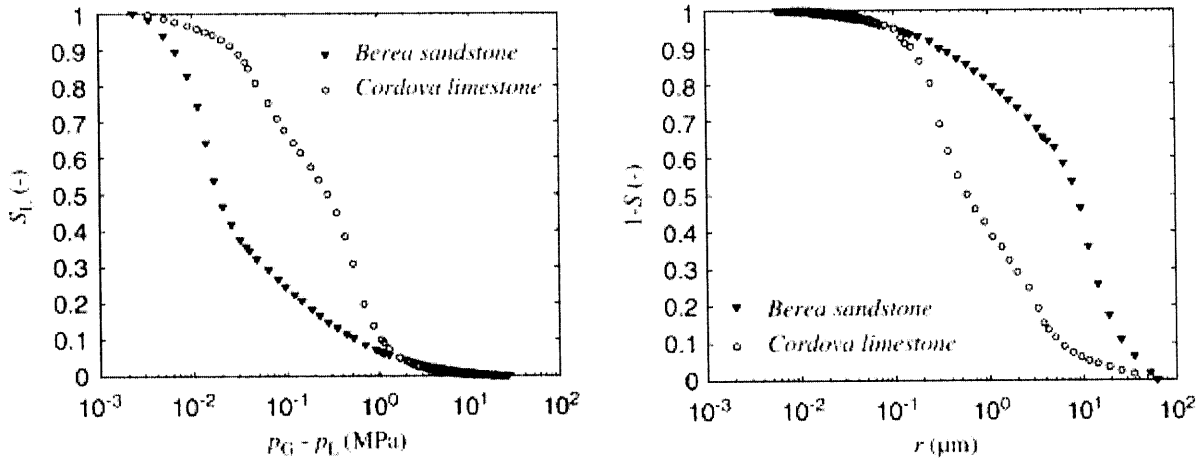

Figure 11: The left figure shows S_L vs the pressure difference, the right figure shows saturation versus radius.

The saturations, S_L, S_G, and S_C versus humidity are shown in Figure 12 for the 5th drying cycle, the drying period when crystals start forming as soon as the drying period begins. In Figure 13, the crystal saturation, S_C is plotted as a function of relative humidity for n successive drying periods.

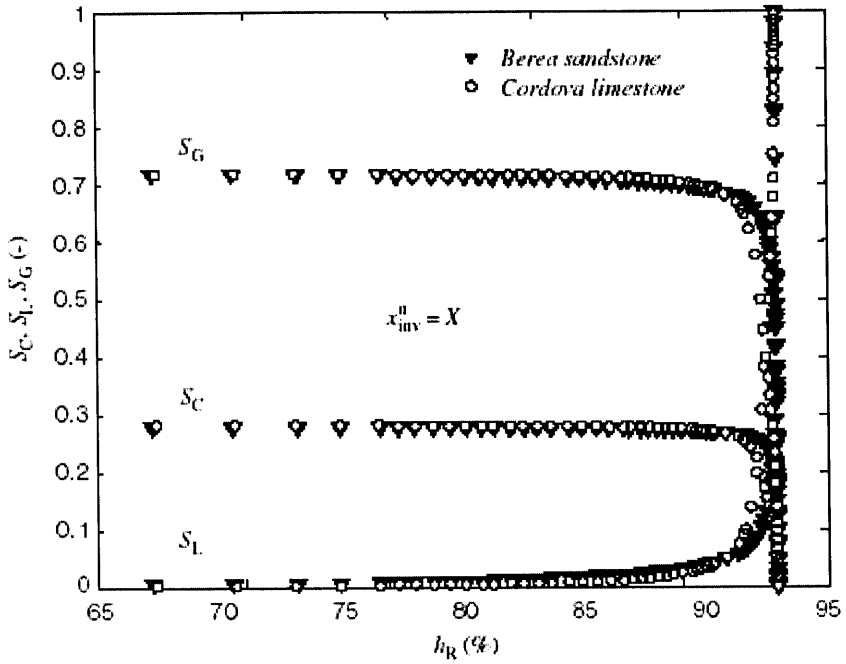

Figure 12: Crystal, liquid, and gaseous saturations versus relative humidity for the 5th drying cycle [1].

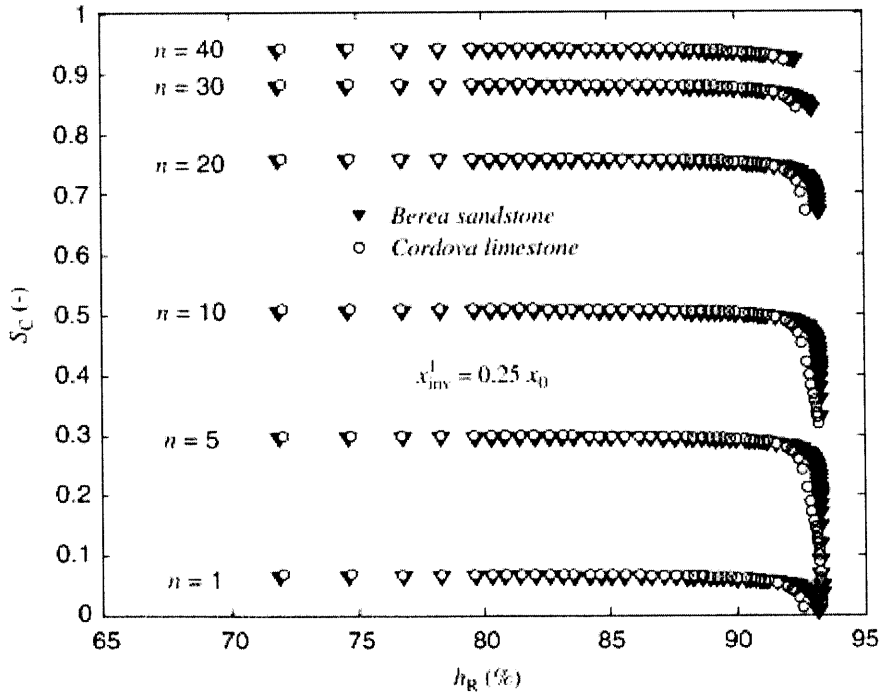

Figure 13: The crystal saturation as a function of relative humidity shown for n drying cycles.

The saturations as a function of humidity for n drying periods that are calculated from Equation (30) are ultimately used to estimate critical stresses that could lead to fracture [1]. The criterion for fracture is derived by setting $p_J - p_0 = s_{ij} = 0$ in Equation 12, obtaining [1]:

$$W = \frac{1}{2}\frac{\sigma^2}{K}. \tag{34}$$

Solving for σ in Equation 34, yields the failure criterion of the form:

$$\varpi = \varpi_{cr} = \sqrt{2KW_{cr}}, \tag{35}$$

where K is the fracture toughness of the material and W_{cr} is the critical threshold beyond which brittle materials cannot store anymore free energy, ϖ is the relative humidity-dependent pressure defined by [1]:

$$\varpi = \frac{RT}{v_W}\left|\ln\frac{h_R}{1-Nx}\right|x\sqrt{\eta(h_R)}, \tag{36}$$

where,

$$\eta(h_R) = \left(\frac{\gamma_{CL}}{\gamma_{GL}} - 1\right)^2 \eta_{CC} - 2\left(\frac{\gamma_{CL}}{\gamma_{GL}} - 1\right)\eta_{CL} + \eta_{LL}, \tag{37}$$

where η_{CL} is given by:

$$\eta_{CL} = b_K b_J + \frac{K}{N_{KJ}}, \tag{38}$$

where the Biot coefficients b_J, the bulk modulus K, and the Biot Modulus N, are macroscopic properties that have been derived by upscaling from a knowledge of microscopic properties and making various approximations [1]. To calculate the macroscopic properties in Equation (38), the current saturations obtained from Equation (30), as well as the porosity of the porous material are required. The calculated pressure ϖ for successive imbibition-drying cycles are plotted versus the relative humidity in Figure 14.

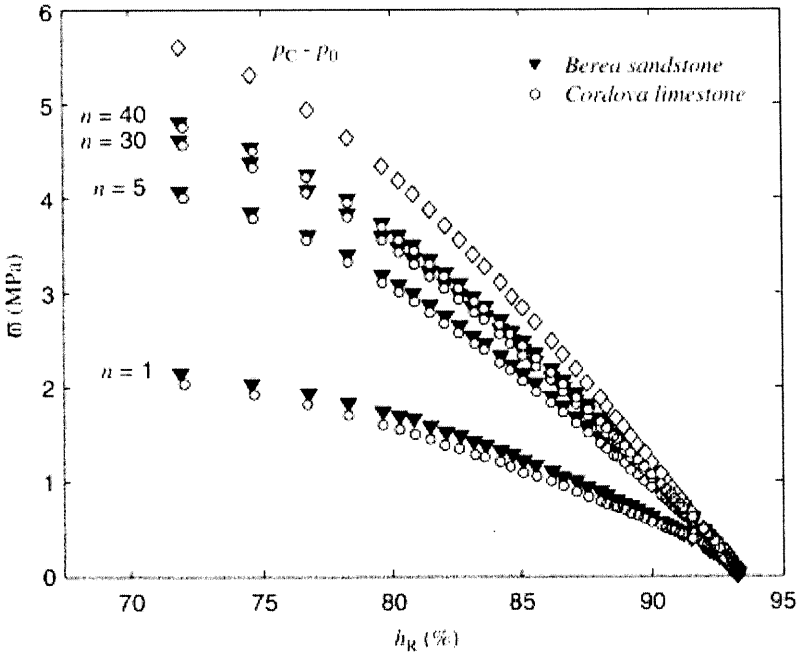

Figure 12: Relative humidity dependent pressures ϖ for successive imbibition-drying cycles versus the relative humidity [1].

From Figure 14 it can be seen that the pressure continually increases both as humidity falls, and as the number of cycles increases. Fracture will occur when pressure ϖ reaches the critical threshold ϖ_{cr} of the material, as defined by Equation (35).

5.3.2 Open Questions

In the case of sodium sulfate, it has been shown experimentally that the most damage occurs during the wetting phase [5]. Yet, Coussy [1] develops his theory of fracture with

respect to crystal growth during drying. But Coussy made the assumption of reversibility when characterizing the crystallization in porous materials as a poroelastic problem. That is, a poroelastic classification requires the dissipation in the process to be equal to zero, and thus, with this assumption on can obtain stresses from the drying cycle and apply them to a wetting cycle. However, this assumption is likely to contribute to inaccuracies, since it has been shown that saturation curves differ significantly during drying and wetting cycles [5], [11].

In addition to the limitation resulting from the assumption of elasticity, the imbibition-drying model [1] does not address temperature variations.

5.4 Length Scale

The length between pores in connection with crystallization and subsequent fracture is a factor that was not explored in the literature. Length scale can be introduced into Coussy's [1] critical stress given by Equation (35), where

$$W_{cr} = \sqrt{\frac{G_f}{L}}, \tag{39}$$

where G_f is the fracture energy [10], giving the critical stress as:

$$\varpi_{cr} = \sqrt{\frac{2EG_f}{L}}, \tag{40}$$

where E is the Young's Modulus. Thus the critical stress is shown to have an inverse relationship with length.

5.5 Incorporating Temperature into Imbibition-Drying Cycles

From Flatt [4] it is clear that temperature drops affect the solubility of saline solution which in effect impacts when supersaturation will occur, which in turn is related to

fracture. These temperatures can be incorporated into Coussy's imbibition-drying model [1] by obtaining different temperatures curves for the molar fraction, x, by assigning different solubility values in Equation (22) (see Figure 15). Furthermore, with changes in the molar fraction, the entry radius r (as a function of humidity) would vary as well (see Figure 16), and more importantly, the molar fraction and the entry radius both come into play in predicting saturations during imbibition-drying cycles, which in turn affects the humidity-dependent pressure, ϖ, and finally the risk of fracture, as defined (e.g., by Equation (35)).

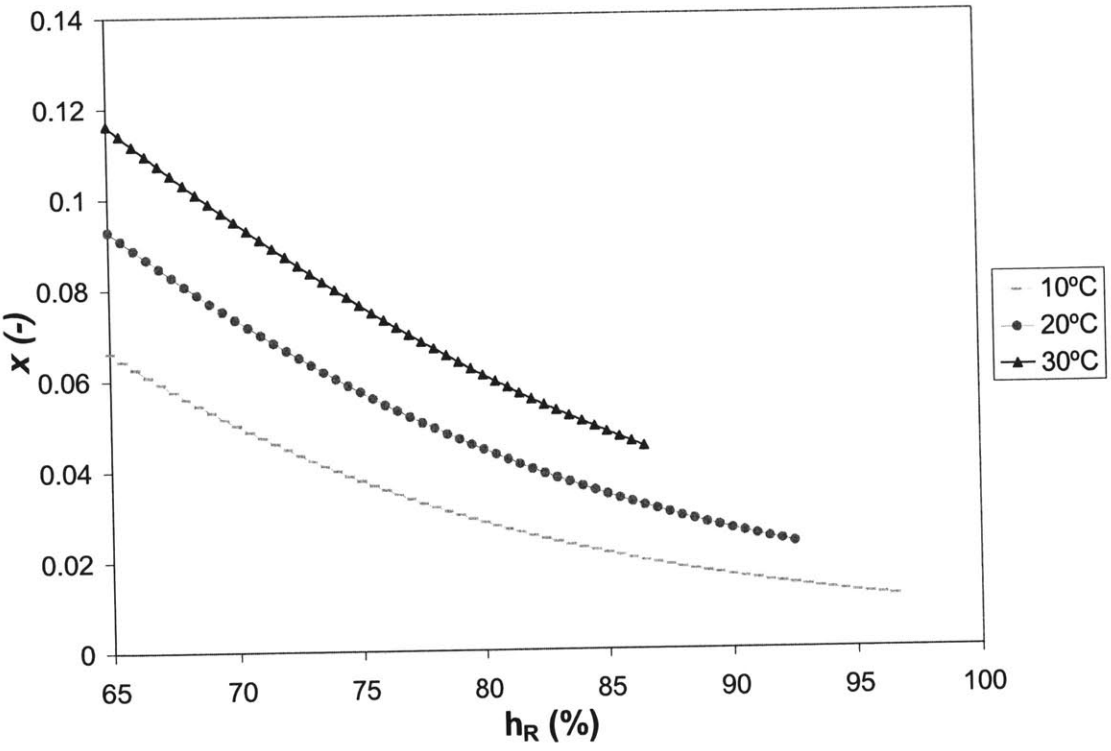

Figure 13: The molar fraction versus relative humidity for temperatures ranging from 10°C to 30°C. Coussy [1] only considers the molar fraction at 20°C (the center curve).

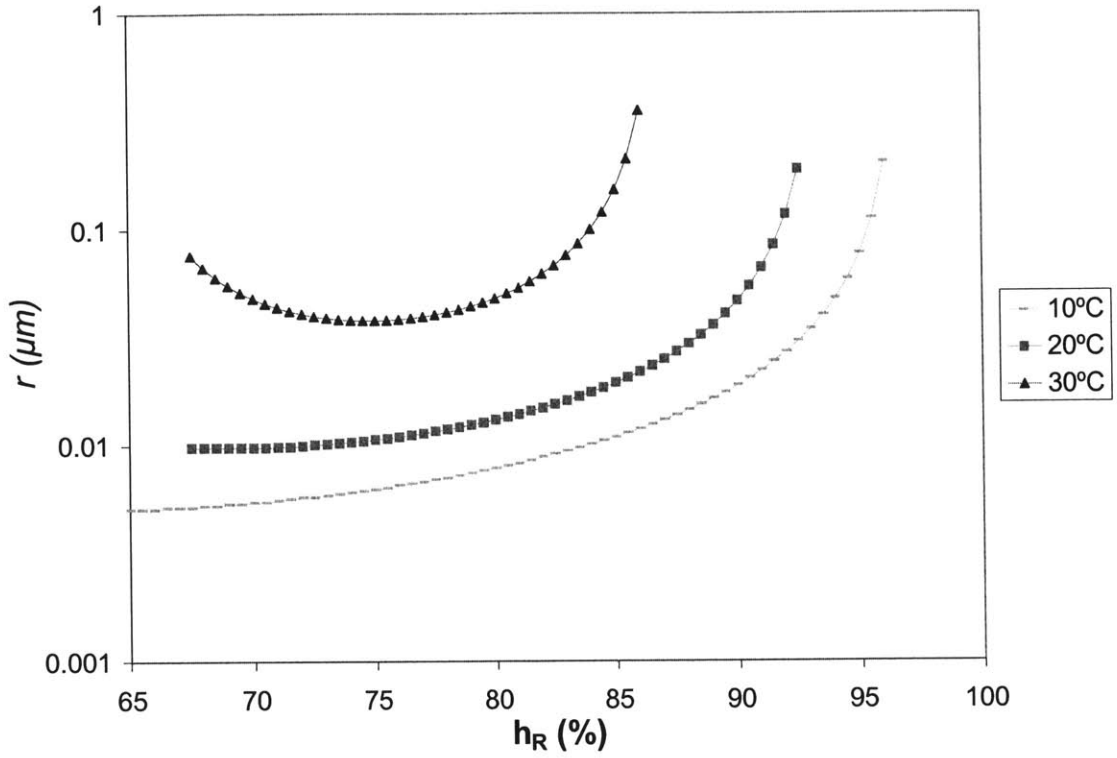

Figure 14: The entry radius versus relative humidity for temperatures ranging from 10°C to 30°C. Coussy [1] only considers the radius at 20°C (the center curve).

5.6 Assembling the Research

The flow chart shown in Figure 17 completes the flow chart shown in Figure 4. That is, Figure 17 represents the step depicted with a question mark. The dotted arrows represent links that have been proposed in this thesis but have not been directly made in the literature. The bottom rectangle refers to Scherer's conclusion that fracture will occur only after crystallization propagates through a large enough region [8]. The propagation of the crystallization requires pervasiveness of high supersaturations (depicted by the center octagon) which can be attained through temperature variations [4] or inhibition drying cycles [1], with pore size [1] and potentially length scale playing a role as well. The entry radius, the pore size, and humidity are all crucial elements contributing to the imbibition-drying cycling [1], with temperature and length scale potentially coming into the picture as well.

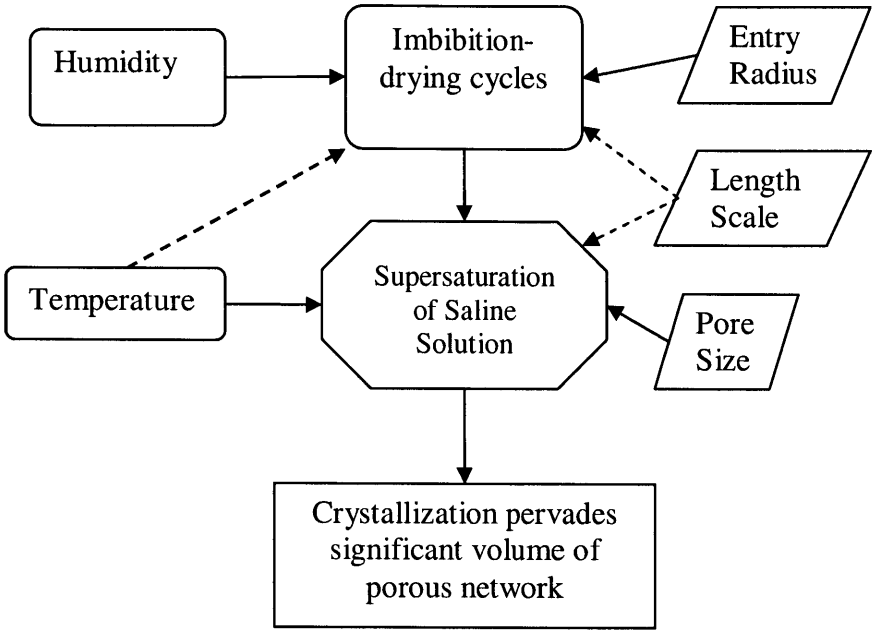

Figure 15: The missing part of the flow chart displayed earlier (see Figure 4) showing the factors leading to fracture.

5.7 Summary

For fracture to occur, Scherer [8] proposes that first crystallization has to spread through a large region of the porous network. This chapter delved into the different ways by which crystallization of salt could spread through a porous network as explored by several researchers. Furthermore, suggestions were made on how to integrate the research into one unified theory as well as to account for elements that have not yet been fully explored. The final chapter will provide suggestions for further research of these elements, as well discuss the practical applications of this research.

Chapter 6

Conclusions

6.1 Introduction

This chapter will discuss the implications of this thesis by first providing suggestions for further research, then addressing the practical applications of this research, and finally presenting an overall summary of the conclusions reached in this thesis.

6.2 Suggestions for Future Research

In section 5.5, it was proposed that temperature be introduced as a factor affecting the results of imbibition-drying cycles. Though it was shown how temperature affects the molar fraction curve as well as the entry radius, it was not quantitatively demonstrated how temperature would actually affect the stress induced by the drying cycles. Furthermore, the effects of length scale need further analysis.

6.3 Application for the Preservationists

Scherer [7] showed that when the contact angle between the crystal and pore wall is small, the stress is small. This would suggest that if the contact angle could be reduced, one could reduce stresses and ensuing damage from crystallization of salt. One way of reducing the contact angle would be to apply a coating to the pores that would in effect reduce the contact angle [7]. Additionally, from Scherer's conclusion that the crystallization pressure is smaller for large pores one could infer that structures made of materials having larger pores should suffer less damage than those with relatively smaller pores.

Preventing repeated cycles drying and imbibition [1] or dissolution and precipitation [4] can help avoid further damage to the material. This would require

knowledge of the salts and the process regarding how they dissolve/precipitate as a function of humidity. However, to prevent such cycles, it would be necessary to place the structure in a controlled environment [4], something that is not always practical.

6.4 Summary

This thesis provides an overview of relevant research related to the crystallization of salt in porous materials. Undoubtedly, much progress has been made in understanding and quantifying the damage resulting from penetration of saline solution into porous materials. However, the formulation of quantifying the factors that lead to fracture remains incomplete. While a number of researchers have focused on different aspects of this process, there is need for one unified theory combining all elements involved. Chapter 5 of this thesis suggests a starting point towards the development of a unified and complete analysis of fracture of porous materials.

References

[1] Coussy, O., 2006. Deformation and brittle fracture from drying-induced crystallization of salt, *Journal of the Mechanics and Physics of Solids*, unpublished manuscript.

[2] DiCarlo, D.A., Bauters, T.W.J., Darnault, C.J.G., Steenhuis, T.S., Parlange, J.-Y., 1999. Lateral expansion of preferential flow path in sands. *Water Resour. Res.* 35 (2), 427–434.

[3] Feilden, Bernard M., 2003. *Conservation of historic buildings.* Burlington, MA: Architectural Press.

[4] Flatt, R., 2002. Salt damage in porous materials: how high supersaturations are generated, *Journal of Mechanics and Physics of Solids,* In Press.

[5] Price, C.A., 1978. The use of the sodium sulfate crystallization test for determining the weathering resistance of untreated stone, *Deterioration and Protection of Stone Monuments*, RILEM, Parias, pp. Price-1 - Price-24.

[6] Rodriguez-Navarro, C., Doehne, E., 1999. Salt Weathering: influence of evaporation rate, supersaturation and crystallization pattern, *Earth Surf. Process. Landforms*, 24, 191-209.

[7] Scherer, G.W., 1999. Crystallization in pores, *Cement and Concrete Research 29*, 1347 – 1358

[8] Scherer, G.W., 2004. Stress from crystallization of salt, *Cement and Concrete Research*, 1613-1624.

[9] Shah, S.P., Swartz, S.E., Ouyang, C., 1995. *Fracture Mechanics of Concrete.* New York: Wiley.

[10] Ulm, F.-J., 2006. *Durability Mechanics – Class Notes 1.570.* MIT.

[11] Xie, M., Agus, S., Schanz, T., Kolditz, O., 2004. An upscaling method and numerical modelling of swelling/shrinking processes in compacted bentonite/sand mixtures. *International Journal for Numerical and Analytical Methods in Geomechanics* 28 (15), 1479-1502.

Appendix A

Matlab code

```
function f = thefunction(x,h)
w=10;           %stoichemtic constant
N=3;
vc=.000220;     % nu c
vw=.000018;     % nu W
d=-.0497;       %  del (dilation factor)
c=.1;           % gamma cl, interfacial energy
g=.072;         % gamma gl
x0=.02235;      % xo
% x0array=[.0113,.02235,.04428];

f=((h/(1-N*x))^((vc/vw)*(d+c/g)))*((x/x0)^N)*(((1-N*x)/(1-N*x0))^w)-1;

harray =[];     % humidity
xarray=[];      % x values obtained by solving eq. 72
rarray=[];      % r values obtained by solving eq. 73

%---------begin solving eq. 72 (Coussy [1]) ----------

for h = 0.65:0.005:0.925
    x = fsolve(@thefunction, 0.02, [], h);
    harray = [harray; h];
    xarray = [xarray; x];
end

w=10;          %stoichemtic constant
N=3;
vc=.000220;     % nu c
vw=.000018;     % nu W
x0=.02235;
d=-.0497;       %  del (dilation factor)
c=.1;           % gamma cl, interfacial energy
g=.072;         % gamma gl
```

```
R=8.314;
T=293.15;


for n=1:1:56
    x=xarray(n);
    r=1/(R*T/(2*vc*(c+d*g))*log(((x/x0)^N)*((1-N*x)/(1-N*x0))^w));
    rarray = [rarray; r];
end


plot(harray*100,xarray)
xlabel ('h_R (%)');
ylabel ('x (-)');

figure
plot(harray*100,rarray*10^6)
xlabel ('h_R (%)');
ylabel ('r (\mum)');
```

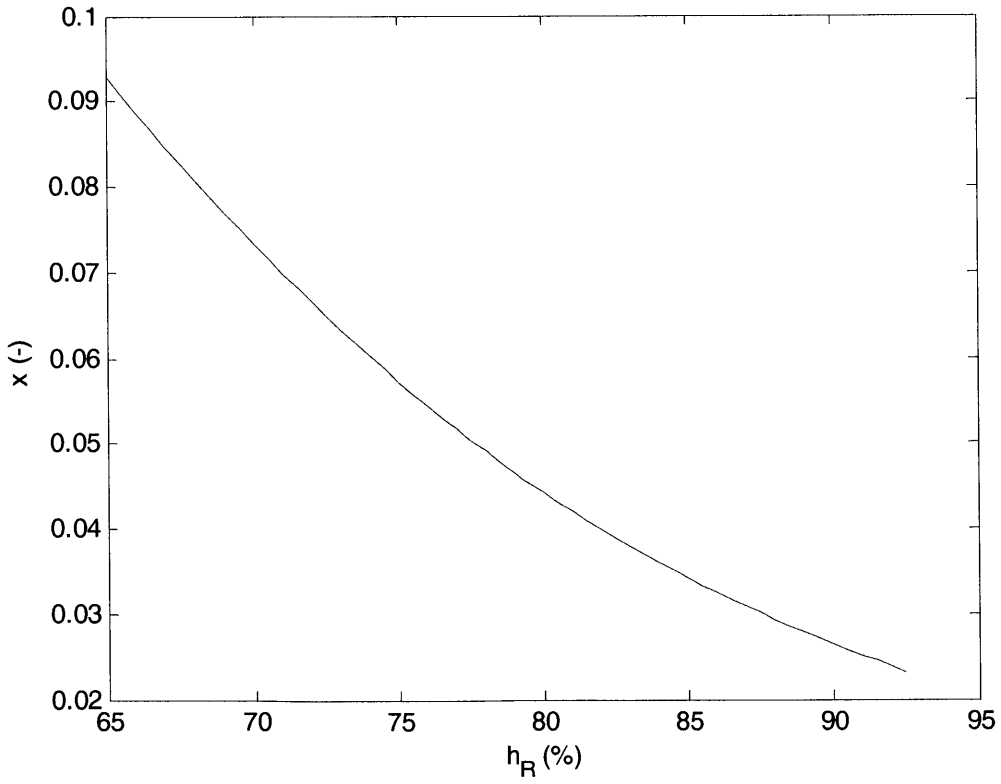

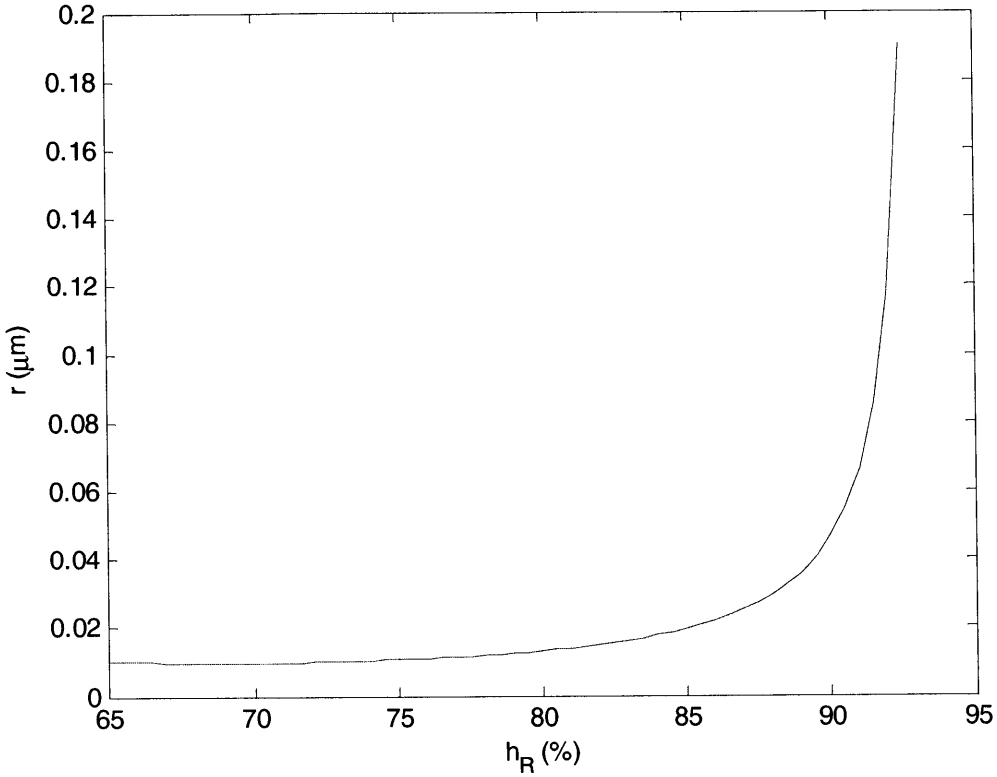
0.2
0.18
0.16
0.14
0.12
0.1
0.08
0.06
0.04
0.02
0
r (μm)
65
70
75
80
85
90
95
h_R (%)

Appendix B

From Flatt [1]: properties of mirabilite, sandstone, and limestone.

Table 1
Main properties of mirabilite

Composition	$\prod_{s(c)} A_{r_a}^{a} \cdot \nu_w H_2O = Na_2SO_4 \cdot 10H_2O$
Stoichiometry	$\nu_{Na^+} = 2,\ \nu_{SO_4^{2-}} = 1,\ \nu_w = 10;\ N = 3$
Molar volumes	$v_C = 220\,cm^3 \cdot mol^{-1};\ v_W = 18\,cm^3 \cdot mol^{-1}$
Solubility at 20 °C	$x_0 = 2.235 \times 10^{-2}$ (Flatt, 2002)
Relative humidity at $p_L = p_0$	$h_R^0 = 1 - Nx_0 = 93.295\%$
Crystallization dilation coefficient	$\delta = -4.97 \times 10^{-2}$ from Flatt (2002)
Crystal–liquid interfacial energy	$\gamma_{CL} = 0.1\,J \cdot m^{-2}$ (Scherer, 1999)

Table 2
Properties of the Berea sandstone and the Cordova limestone

Matrix properties	Berea sandstone	Cordova limestone
Bulk modulus k_s	28.9 GPa (Hart and Wang, 1995)	72.6 GPa (Hart and Wang, 1995)
Shear modulus g_s	1.54 GPa (Hart and Wang, 1995)	3.59 GPa (Hart and Wang, 1995)
Poisson coefficient ν_s	0.474	0.476
Stone properties		
Porosity ϕ_0	0.228	0.257
Empty bulk modulus K	5.3 GPa	11 G Pa
Biot coefficient b	0.817	0.848
Pore size distribution $S(r)$	See Fig. 1	See Fig. 1
Maximum radius r_{max}	62 μm	52 μm
Molar fraction X	2.2357×10^{-2}	2.2353×10^{-2}

The values for the matrix moduli are derived by using the experimental data given in Hart and Wang (1995), and inverting relations (77) and (78).